Elasticity of adhesion bonds determines multistable mechanosensitive behaviour of living cells.

Ping Liu,[1] Qiuyu Wang,[1,2] Mingxi Yao,[3,*] and Artem K. Efremov[1,†]

[1] *Institute of Systems and Physical Biology, Shenzhen Bay Laboratory, Shenzhen, China 518132*
[2] *School of Biological Sciences, The University of Hong Kong, Hong Kong SAR, China 999077*
[3] *Department of Biomedical Engineering, Southern University of Science and Technology, Shenzhen, China 518055*

(Dated: September 4, 2023)

The ability of cells to sense the mechanical properties of their microenvironment is essential to many physiological processes. Previously, the molecular clutch theory was developed to explain many mechanosensitive cell behaviours. However, because it does not take into account the nonlinear elastic properties of key proteins involved in the formation of cell adhesion complexes, this theory cannot establish a relationship between mechanosensitive cell adhesion behaviour and the force response of underlying proteins observed in single-molecule experiments. In this study, we developed a model incorporating the experimentally measured nonlinear elastic properties of such proteins to investigate their influence on cell adhesion behaviour. It was found that the model not only could accurately fit previous experimental measurements of the cell traction force and the retrograde actin flow, but also predicted multistable cell adhesion behaviour along with a feedback loop between the densities of the extracellular matrix proteins and myosin II motors in living cells. Existence of the latter was successfully confirmed in experiments on NIH-3T3 cells. Taken together, our study provides a theoretical framework for understanding how the mechanical properties of adapter proteins, local substrate deformations and myosin II contractility affect cell adhesion behaviour across different cell types and physiological conditions.

Keywords: Cell mechanosensing, cell adhesion, molecular clutch, talin, integrin

INTRODUCTION

The main distinguishing feature of living organisms is their ability to perceive and adapt to the surrounding environment. As such, living cells are able to sense and respond to mechanical cues, changing their behaviour depending on the substrate rigidity and topography [1]. Mechanosensory perception of living cells is important for regulation of many physiological processes, including cell migration, proliferation, differentiation and apoptosis [2]. Moreover, cell mechanosensing plays a central role in various pathological conditions such as fibrosis, cancer, and cardiovascular diseases [3]. A better understanding of cell mechanosensing mechanisms could lead to deeper insights into these processes.

At the molecular level, mechanosensing processes are mediated by a number of proteins, including p130cas, talin, α-catenin, and ion channels such as Piezo 1/2, that transduce mechanical cues into biochemical signals, which activate downstream signalling cascades [4, 5]. While single-molecule force spectroscopy techniques have greatly improved our understanding of the mechanosensing mechanisms of such proteins [6], much less is known about how their force-dependent response is integrated at the mesoscale level, ultimately directing cell behaviour.

To address this complex problem, various theoretical models have been previously proposed. Among them, the molecular clutch theory has proven to be one of the most successful in explaining a wide range of mechanobiology phenomena such as filopodia extension, traction force generation, and cell spreading [7–12]. It has been suggested that cells form highly dynamic adhesion links (so-called molecular clutches) between the actin cytoskeleton and extracellular matrix (ECM) through interactions of adaptor proteins with transmembrane adhesion receptors and the actin cytoskeleton [Figure 1(a)], which give rise to a traction force that allows propagation of the leading edge of the cell during cell spreading and migration [7, 8]. Furthermore, it has been hypothesised that substrate stiffness can potentially modulate tension build-up and lifetime of the molecular clutches through force-dependent changes in bond dissociation rates, providing explanation for the mechanosensitive behaviour of cell adhesion [8–12].

However, despite its success, current implementations of molecular clutch model still have several limitations. First, the existing molecular clutch models do not account for local deformations of the substrate at the adhesion sites of molecular clutches, considering only the overall average substrate deformation over a large cell adhesion area encompassing many molecular clutches [9–13]. Meanwhile, the theory of elasticity predicts that the local substrate deformations are orders of magnitude greater than the average value. Second, it is known that *in vivo* the ECM usually consists of heterogeneous fibrous substrates such as fibronectin and collagen that are highly deformable at nanometer scales. Thus, a more explicit treatment of molecular clutch model that account for these local deformations could better describe the physiological conditions.

In addition, in order to capture the effect of substrate

* Corresponding author e-mail: yaomx@sustech.edu.cn
† Corresponding author e-mail: artem@szbl.ac.cn

elasticity on cell mechanotransduction, existing models often assume that the stress experienced by adhesion bonds is mainly determined by substrate deformations. As a result, the stiffness of molecular clutches is usually set to a very high value, ignoring all previous measurements made in single molecular experiments. For example, in ref. [11], the spring constant of the molecular clutches was set to 1 nN/nm in order to fit experimental data, which is three to four orders of magnitude greater than the experimentally measured stiffness of adaptor proteins such as talin, α-catenin or vinculin ($\sim 0.1 - 0.5$ pN/nm [14–16]). Clearly, this limits the capability of the existing molecular clutch models to fully grasp the physiological picture underlying the mechanosensitive behaviour of cell adhesion.

Finally, it should be noted that proteins composing molecular clutches serve as integral mediators of cell mechanotransduction, and besides the well-studied talin, there are many other adapter proteins that have interaction sites for both actin and adhesion receptor that can potentially act as molecular clutch proteins in various physiological contexts. Examples include Shootin1, associated with axon guidance, which interacts with the actin cytoskeleton and L1-CAM adhesion receptor [17]; tensins, which are prevalent in mature cell adhesions and connect the actin cytoskeleton to integrins [18]; and the Abl family of tyrosine kinases, which also localize at cell adhesions, interacting with actin filaments and adhesion receptors [19]. The diverse mechanical properties of these proteins suggest that the regulation of cell adhesion behaviour may be highly context dependent, being influenced by a specific adapter protein involved. This underlines the necessity to incorporate this diversity in our understanding of mechanobiology and its role in physiological and pathological conditions.

To address the above issues and to gain deeper insights into the origin of highly nonlinear response of cell adhesion to mechanical properties of the ECM, we developed a new semi-analytical approach based on consideration of the long-term behaviour of molecular clutches, incorporating into the model experimentally measured force-response of adapter proteins and local substrate deformations at the adhesion sites of the molecular clutches. This made it possible to accurately fit previously published experimental data and construct a simple geometric interpretation of the dynamic behaviour of the molecular clutch system, which revealed that the latter undergoes a series of bifurcations that have a strong effect on cell adhesion. Namely, it was found that these bifurcations result in a high sensitivity of cell behaviour to the elastic properties of molecular clutches and the contractile activity of myosin II motor proteins, thus giving new insights into the potential biological functions of these proteins. Lastly, the developed model predicted the existence of a molecular pathway responsible for the regulation of the number of myosin II motors near the cell-substrate interface in response to changes in the fibronectin density, which was experimentally confirmed in our study.

METHODS

Linear molecular clutch model

To describe the dynamics of the molecular clutch system shown in Figure 1(b), we considered formation / dissociation kinetics of molecular clutches under mechanical load (F) generated by myosin II motors. In the model, all potential sites for clutch formation were divided into two groups: those occupied by clutches ('on' state) and those which are not ('off' state). Accordingly, the state of the entire system was represented by a time-dependent probability distribution, $p_{\mathrm{on}}(l,t)$, to observe an engaged molecular clutch with the mechanical strain l at time t at the sites available for the formation of molecular clutches. It is clear that this distribution must satisfy the following normalization condition:

$$p_{\mathrm{off}}(t) + \int_{-\infty}^{\infty} p_{\mathrm{on}}(l,t)\,\mathrm{d}l = 1 \tag{1}$$

Where $p_{\mathrm{off}}(t)$ is the time-dependent probability of the off-state.

While immediately after assembly molecular clutches are in a mechanically relaxed state, the retrograde flow of actin filaments created by myosin II motors leads to their gradual stretching. This results in increase of the mechanical strain (l) of molecular clutches, causing their subsequent dissociation. Thus, Eq. (1) must be supplemented by the following boundary conditions:

$$p_{\mathrm{on}}(l<0,t) = p_{\mathrm{on}}(+\infty,t) = 0 \tag{2}$$

To describe dissociation kinetics of molecular clutches, it was assumed in this study that this process is mainly driven by detachment of integrins from their ECM ligands, such as fibronectin. Indeed, previous studies suggest that this may be the weakest point of molecular clutches, as bonds between other molecular clutch components appear to be strongly enhanced by applied mechanical load [20, 21]. Since integrin-ECM bonds have previously been shown to possess intermediate catch-bond behaviour [22], the dissociation rate of molecular clutches (k_{off}) was approximated by the following double-exponential formula that fits the experimental data fairly well [Figure S1, SI]:

$$k_{\mathrm{off}}(F) = k_{\mathrm{off}}^{0}\, e^{F/F_{\mathrm{d}}} + k_{\mathrm{off}}^{0'}\, e^{F/F_{\mathrm{d}}'} \tag{3}$$

Where F is the tension of the bond. F_{d} and F_{d}' are the characteristic dissociation forces of the catch-bond, and k_{off}^{0} and $k_{\mathrm{off}}^{0'}$ are the dissociation rates at zero mechanical load.

As for k_{on} rate, since it was assumed that immediately after assembly molecular clutches are in a mechanically relaxed state with zero mechanical strain, then:

$$k_{\mathrm{on}}(l) = k_{\mathrm{on}}\delta(l) \tag{4}$$

Where k_{on} is a fixed constant and $\delta(l)$ is the Dirac δ-function.

Finally, following previous studies [8–12], the resisting effect of the clutch tension on the movement rate of myosin II motors (v) was approximated by a linear force-velocity relation:

$$v = v_0 \left[1 - \frac{F_\mathrm{c}}{N_\mathrm{m} F_\mathrm{st}}\right] \tag{5}$$

Here F_c is the total tension of the engaged molecular clutches. F_st is the stalling force of a single myosin II motor. v_0 is the movement rate of myosin II motors at zero mechanical load. N_m is the total number of myosin motors pulling actin filaments in a cell adhesion area. Since previous studies suggest that myosin II motors have a rather local effect on the actin cytoskeleton [23], N_m was approximated as: $N_\mathrm{m} = \pi R^2 \sigma_\mathrm{m}$, where σ_m is the density of myosin II motors near the cell-substrate interface and R is the characteristic radius of cell adhesion areas ($R \approx 1.7\ \mu$m [11]).

By combining the formulas above, it can be shown that the dynamics of the molecular clutch system can be described by the following master equation:

$$\begin{cases} \dfrac{\partial p_\mathrm{on}(l,t)}{\partial t} = -k_\mathrm{off}(l)\, p_\mathrm{on}(l,t) + k_\mathrm{on}(l)\, p_\mathrm{off}(t) - \\ \qquad\qquad - \left[v(t) - \dfrac{\partial x_\mathrm{s}(t)}{\partial t}\right] \dfrac{\partial p_\mathrm{on}(l,t)}{\partial l} \\ \dfrac{\partial p_\mathrm{off}(t)}{\partial t} = \displaystyle\int_0^\infty \Big[k_\mathrm{off}(l)\, p_\mathrm{on}(l,t) - k_\mathrm{on}(l)\, p_\mathrm{off}(t)\Big]\, \mathrm{d}l \\ \dfrac{\partial x_\mathrm{s}(t)}{\partial t} = \dfrac{1}{\xi_\mathrm{s}}\Big[F_\mathrm{c}(t) - k_\mathrm{s} x_\mathrm{s}(t)\Big] \\ F_\mathrm{c}(t) = N_\mathrm{c} \displaystyle\int_0^\infty F(l)\, p_\mathrm{on}(l,t)\, \mathrm{d}l \\ v(t) = v_0 \left[1 - \dfrac{F_\mathrm{c}(t)}{N_\mathrm{m} F_\mathrm{st}}\right] \end{cases} \tag{6}$$

Here $k_\mathrm{off}(l) = k_\mathrm{off}(F(l))$, where $F(l) = k_\mathrm{c} k_\mathrm{s}' l/(k_\mathrm{c} + k_\mathrm{s}')$ is the strain-dependent tension of molecular clutches. k_c and k_s' are the spring constants of the cellular and extracellular parts of molecular clutches, respectively [see Figure 1(b)]. $N_\mathrm{c} = \pi R^2 \sigma_\mathrm{c}$ is the maximum number of molecular clutches that can form in a cell adhesion area, where σ_c is the surface density of sites available for the formation of molecular clutches. $x_\mathrm{s}(t)$ is the large-scale mechanical deformation of the substrate [Figure 1(b)]. ξ_s and k_s are constants describing the viscous and elastic properties of the substrate.

The main difference between k_s' and k_s spring constants is that k_s' describes the average local deformation of the substrate at the adhesion site of a single molecular clutch due to the pulling force generated by this clutch; whereas k_s spring constant describes the average substrate deformation over a much larger area of cell adhesion of the radius R that encompasses many molecular clutches.

Using the theory of elasticity, it can be shown that [24]:

$$k_\mathrm{s}' = \frac{4\pi r E}{9} \quad \text{and} \quad k_\mathrm{s} = \frac{4\pi R E}{9} \tag{7}$$

Where E is the Young's modulus of the substrate and r is the characteristic radius of the adhesion site of a single molecular clutch.

Since experimental studies show that actin filaments exhibit retrograde movement at nearly constant rates [$v(t) \approx$ const] [8, 11, 23, 25], it is clear that myosin II motors and the entire ensemble of molecular clutches function close to a steady-state. This makes it possible to considerably simplify the above master equation. Namely, from the last row of Eq. (6) it follows that $v(t) \approx$ const implies that $F_\mathrm{tot}(t) \approx$ const. Then from the third line it can be concluded that $x_\mathrm{s}(t) \approx$ const as soon as $t \gg \xi_\mathrm{s}/k_\mathrm{s}$. Finally, since the probability distribution $p_\mathrm{on}(l,t)$ is bounded by 0 and 1, we can apply time-averaging to the first two rows of the master equation over a sufficiently long time period, T, leading to nullification of the left sides of these two rows. As a result, it can be concluded that the long-term behaviour of the molecular clutch system corresponds to the stationary solution of Eq. (6), which is described by the following system of equations:

$$\begin{cases} \dfrac{\partial p_\mathrm{on}(l)}{\partial l} = -\dfrac{k_\mathrm{off}(l)}{v}\, p_\mathrm{on}(l), \ \text{for } l > 0 \\ \displaystyle\int_0^\infty k_\mathrm{off}(l)\, p_\mathrm{on}(l)\, \mathrm{d}l = p_\mathrm{off}\, k_\mathrm{on} \\ F_\mathrm{c} = N_\mathrm{c} \displaystyle\int_0^\infty F(l)\, p_\mathrm{on}(l)\, \mathrm{d}l \\ F_\mathrm{c} = F_\mathrm{m} = N_\mathrm{m} F_\mathrm{st} \left[1 - \dfrac{v}{v_0}\right] \\ x_\mathrm{s} = \dfrac{F_\mathrm{c}}{k_\mathrm{s}} \end{cases} \tag{8}$$

Here $p_\mathrm{on}(l) = \langle p_\mathrm{on}(l,t)\rangle_T$ is the time-averaged probability distribution. F_m is the total pulling force generated by myosin II motors.

It is straightforward to solve Eq. (8) by parts by noting that the solution can be obtained as an intersection of $F_\mathrm{c}(v)$ and $F_\mathrm{m}(v)$ graphs. This makes it possible not only to construct a simple geometric interpretation of solutions of Eq. (8), but also to assess their stability, see Appendix A and Figure S4, SI.

While $F_\mathrm{m}(v)$ can be directly obtained from the third row of Eq. (8), calculation of $F_\mathrm{c}(v)$ requires knowledge of $p_\mathrm{on}(l)$ probability distribution, which can be found from the first two rows of Eq. (8):

$$p_\mathrm{on}(l) = \frac{k_\mathrm{on}\, e^{-\frac{1}{v}\int_0^l k_\mathrm{off}(l')\,\mathrm{d}l'}}{\displaystyle\int_0^\infty \Big[k_\mathrm{on} + k_\mathrm{off}(l)\Big]\, e^{-\frac{1}{v}\int_0^l k_\mathrm{off}(l')\mathrm{d}l'}\, \mathrm{d}l} \tag{9}$$

Knowing $p_\mathrm{on}(l)$ distribution, one can easily obtain the total tension of the engaged molecular clutches (F_c) from Eq. (8) and the traction stress (P) exerted by a cell to the substrate:

$$P = \frac{F_\mathrm{c}}{\pi R^2} \tag{10}$$

In the special case of slip-bonds ($k_{\rm off}^{0'} = 0$), Eq. (9) reduces to a simple analytic formula:

$$p_{\rm on}(l) = \frac{\phi(a,\varepsilon)}{\phi(a,\varepsilon)+1}\, e^{a[1-e^{F(l)/F_{\rm d}}]} \tag{11}$$

Leading to:

$$F_{\rm c} = N_{\rm c} F_{\rm d}\, \frac{\phi(a,\varepsilon)}{\phi(a,\varepsilon)+1}\, \frac{a\, G_{2,3}^{3,0}\left(\begin{matrix} 0,\, 0 \\ -1,-1,-1 \end{matrix} \middle| a \right)}{E_1(a)} \tag{12}$$

Where $a = k_{\rm off}^0 F_{\rm d}/k_{\rm c} v$, $\phi(a,\varepsilon) = a e^{\varepsilon + a} E_1(a)$ and $\varepsilon = \ln(k_{\rm on}/k_{\rm off}^0)$. $E_1(a) = \int_a^\infty t^{-1} e^{-t} {\rm d}t$ is the exponential integral function. $G_{p,q}^{m,n}$ is the Meijer's G-function.

Talin molecular clutch model

While in the above model molecular clutches are represented by linear springs, single-molecule experiments show that adapter proteins, such as talin, exhibit highly nonlinear response to stretching force [16]. To account for the observed nonlinear behaviour of talin molecules and force-induced unfolding of mechanosensitive talin domain (R3), the first two rows in Eq. (6) must be replaced by the following matrix equations:

$$\begin{cases} \dfrac{\partial \mathbf{p}_{\rm on}(l)}{\partial l} = \dfrac{1}{v}\mathbf{A}(l)\mathbf{p}_{\rm on}(l), \text{ for } l > 0 \\ \displaystyle\int_0^\infty \mathbf{k}_{\rm off}^T(l)\, \mathbf{p}_{\rm on}(l)\, {\rm d}l = p_{\rm off}\, k_{\rm on} \end{cases} \tag{13}$$

Where

$$\mathbf{p}_{\rm on}(l) = \begin{pmatrix} p_{\rm on}^{\rm f}(l) \\ p_{\rm on}^{\rm u}(l) \end{pmatrix} \quad \text{and} \quad \mathbf{k}_{\rm off}(l) = \begin{pmatrix} k_{\rm off}(l) \\ k_{\rm off}(l) \end{pmatrix}$$
$$\mathbf{A}(l) = \begin{pmatrix} -k_{\rm off}(l) - k_{\rm u}(l) & k_{\rm f}(l) \\ k_{\rm u}(l) & -k_{\rm off}(l) - k_{\rm f}(l) \end{pmatrix} \tag{14}$$

Here $p_{\rm on}^{\rm f}(l)$ and $p_{\rm on}^{\rm u}(l)$ are the time-averaged distribution probabilities of engaged molecular clutches in the case of folded and unfolded mechanosensitive talin domain, respectively. $\mathbf{A}$ is the transition matrix. Superscript T denotes the matrix transpose. $k_{\rm u}$ and $k_{\rm f}$ are the unfolding and refolding rates of the mechanosensitive talin domain.

In the model, $k_{\rm u}$ rate was approximated by the Bell's formula:

$$k_{\rm u}(l) = k_{\rm u}^0 e^{F^{\rm f}(l)/F_{\rm u}} \tag{15}$$

Where $k_{\rm u}^0$ is the unfolding rate of the mechanosensitive talin domain at zero load. $F^{\rm f}(l)$ is the force-extension curve of a molecular clutch in the case of a folded mechanosensitive talin domain. $F_{\rm u}$ is the characteristic unfolding force of the mechanosensitive talin domain.

As for $k_{\rm f}$, it was calculated from the equilibrium constant ($K_{\rm eq}$):

$$K_{\rm eq}(l) = \frac{k_{\rm f}(l)}{k_{\rm u}(l)} = e^{-\Delta G(l)/k_{\rm B}T} \tag{16}$$

Where ΔG is the difference between the free energies of a molecular clutch in the cases of the folded and unfolded mechanosensitive talin domain:

$$\Delta G(l) = -k_{\rm B}T \ln \frac{k_{\rm f}^0}{k_{\rm u}^0} + \int_0^l \Big[F^{\rm f}(l') - F^{\rm u}(l')\Big] {\rm d}l' \tag{17}$$

Here $k_{\rm f}^0$ is the refolding rate of the mechanosensitive talin domain at zero load. $F^{\rm f}(l')$ and $F^{\rm u}(l')$ are the force-extension curves of a molecular clutch in the folded and unfolded states of talin, respectively. To calculate these curves, we used the freely-jointed chain model for the rod part of talin, treating each globular domain as a solid body. As for the talin unstructured peptide linker and unfolded mechanosensitive talin domain, they were described with the help of the worm-like chain model.

To solve Eq. (13), we first applied the Runge-Kutta method to the differential equation from the first row, which describes the evolution of the vector $\mathbf{p}_{\rm on}$ as a function of mechanical strain. To this aim, we used the following boundary condition:

$$\widetilde{\mathbf{p}}_{\rm on}(0) = \frac{1}{k_{\rm f}(0) + k_{\rm u}(0)} \begin{pmatrix} k_{\rm f}(0) \\ k_{\rm u}(0) \end{pmatrix} \tag{18}$$

The resulting solution, $\widetilde{\mathbf{p}}_{\rm on}(l)$, was then renormalized to obtain the final probability distribution, $\mathbf{p}_{\rm on}(l)$, satisfying the first and the second rows of Eq. (13):

$$\mathbf{p}_{\rm on}(l) = \frac{k_{\rm on}\widetilde{\mathbf{p}}_{\rm on}(l)}{\displaystyle\int_0^\infty \Big[(k_{\rm on}, k_{\rm on}) + \mathbf{k}_{\rm off}^T(l)\Big]\, \widetilde{\mathbf{p}}_{\rm on}(l) {\rm d}l} \tag{19}$$

Finally, the traction force generated by engaged molecular clutches was calculated as:

$$F_{\rm c} = \frac{N_{\rm c} \displaystyle\int_0^\infty \mathbf{F}^T(l)\, \mathbf{p}_{\rm on}(l)\, {\rm d}l}{1 - \alpha \displaystyle\int_0^\infty p_{\rm on}^{\rm u}(l)\, {\rm d}l} \tag{20}$$

Where $\mathbf{F}^T = (F^{\rm f}, F^{\rm u})$, and α is a model parameter describing the force-induced reinforcement of cell adhesion sites [26] due to exposure of the talin's cryptic site for vinculin binding [15, 16]. Specifically, α is the average number of new sites available for the molecular clutch formation, which are added to the system upon unfolding of each mechanosensitive talin domain.

More additional details regarding the assessment of the stability of the above mathematical solutions and description of the experimental methods used to validate model predictions can be found in Appendices A and B, SI. The values of the model parameters used in the calculations are listed in Table 1, SI.

RESULTS

Local substrate deformations are important for the mechanosensitive behaviour of cell adhesion

To investigate the potential role of the elastic properties of adapter proteins and local substrate deformations in the regulation of the mechanosensitive behaviour of cell adhesion, we used the model schematically shown in Figure 1(b) in which molecular clutches were represented by springs consisting of two parts: 1) cellular, corresponding to adapter proteins, and 2) extracellular, describing local substrate deformations at the adhesion sites of the molecular clutches.

From the theory of elasticity, it is known that elastic substrate deformations are inversely proportional to the linear size of the adhesion area to which mechanical stress is applied [Eq. (7)]. Taking into account the experimentally measured size of cell adhesion areas (~ 1.7 μm [11]) and the typical size of the binding sites of adhesion receptors (up to several nanometers), it can be concluded that local substrate deformations at the adhesion sites of molecular clutches should be significantly greater than the substrate deformation averaged over a large area of cell adhesion. Thus, local substrate deformations, which are missing in molecular clutch models, should have a much stronger effect on the dissociation kinetics of engaged molecular clutches compared to the average deformation of the substrate, which is usually used to describe the elastic behaviour of the substrate.

Indeed, it can be shown that if the local substrate deformations are completely neglected ($k_s' \to \infty$), the long-term sensitivity of the molecular clutch system to the mechanical properties of the substrate is significantly reduced. Namely, in this case, the probability distribution $p_{\rm on}(l)$ of observing a given site occupied by a molecular clutch with the mechanical strain l becomes independent of the Young's modulus of the substrate [see Eq. (3), Eq. (9) and comments after Eq. (6)]. This result is valid both for the model in which the cellular part of molecular clutches is represented by a linear spring (linear clutch model), and for the model in which it is represented by a nonlinear spring with a talin-like force-response (talin clutch model). Thus, in the absence of local substrate deformations at the adhesion sites of molecular clutches, the molecular clutch system loses its mechanosensitive properties after relaxation to the long-term behaviour, – a paradoxical situation, given that the molecular clutch theory was originally developed to describe the long-term mechanosensitive behaviour of cells observed in experiments. This result highlights the importance of local substrate deformations by molecular clutches, suggesting that cells must be able to pinch the substrate in order to probe and properly respond to its mechanical properties.

Potential effect of the talin force-response on cell adhesion

To test the model developed in our study, we first fitted experimental data on the mechanosensitive behaviour of WT MEF cells and MEF Talin 1 KO, Talin 2 shRNA cells from ref. [11] using the linear clutch model and the talin clutch model. As can be seen from Figures 1(c,d), both models were able to accurately describe the experimental data. Furthermore, almost all of the fitted model parameter values were found to be in good agreement with previous studies [Table 1, SI], suggesting that the models correctly reflect the main physicochemical properties of the molecular clutch elements. Interestingly, the data fitting indicates that in the case of MEF Talin 1 KO, Talin 2 shRNA cells, the cellular parts of molecular clutches are more than ten times stiffer (3.1 pN/nm) compared to the case of WT MEF cells (0.14 pN/nm), suggesting that cells potentially use at least two different types of molecular clutches to establish adhesion bonds with the substrate – soft (talin-based) and rigid.

Furthermore, from Figures 1(c,d) it can be seen that the linear clutch model and the talin clutch model both provide a fairly accurate description of cell adhesion behaviour, raising the question of whether the elastic properties of the cellular part of molecular clutches play any significant role in it.

To answer this question, we investigated the potential contribution of the nonlinear force-response of talin to the elastic properties of molecular clutches. To this aim, we plotted and compared the force-extension curves of linear molecular clutches and nonlinear talin clutches at different values of the substrate Young's modulus (E), see Figure 1(e).

It was found that in the case of $E \leq 10$ kPa, both linear molecular clutches and talin molecular clutches have almost the same force-extension curves, which indicates that the leading role in determining the elastic characteristics of molecular clutches is played not by the cellular, but by the extracellular part of molecular clutches. This explains why both the linear and talin clutch models are in such good agreement with the experimental data collected in $E < 30$ kPa range. On the other hand, Figure 1(e) shows that the nonlinear force-response of talin plays an important role in the case of rigid substrates ($E > 30$ kPa). Thus, it can be concluded that the elasticity of the cellular part of molecular clutches potentially determines the behaviour of cell adhesion on rigid substrates rather than on soft ones.

Indeed, by varying the spring constant of the cellular part of molecular clutches (k_c) in the linear clutch model, it was found that the cell traction curve and the actin flow curve undergo significant changes on rigid substrates, and to a much lesser extent on soft substrates, which confirms the above conclusion, see Figure 2.

Bifurcation of the molecular clutch system causes bistability of cell adhesion on rigid substrates

Interestingly, our model also predicted that at higher values of the spring constant, k_c, the cell traction curve and the actin flow curve undergo a bifurcation, which results in appearance of two additional branches, – a phenomenon that was found to depend on the density of myosin II motors [see Figure 2].

To investigate the stability of these additional branches, as well as the rest of the graphs displayed in Figure 2, we performed a linear stability analysis. Surprisingly, all the graphs turned out to correspond to unstable solutions of Eq. (6) in the case when the Young's modulus of the substrate exceeds $100 - 1000$ Pa, see Appendix A, SI. Yet, it is know from the derivation of Eq. (8) that the long-term behaviour of the molecular clutch system must converge to at least one of the branches of each graph shown in Figure 2. These two seemingly contradictory results can be reconciled only if the molecular clutch system instead of directly converging to a stationary solution of Eq. (6) experiences persistent oscillations around it over time. Using stochastic simulations based on the algorithm described in ref. [10, 11, 13], this model prediction was successfully tested and confirmed, showing that the molecular clutch system does indeed experience oscillations / fluctuations around stationary solutions of Eq. (6), see Figure S3, SI.

Remarkably, unlike the conventional molecular clutch model [8, 12], which exhibits rather strong fluctuations around the stationary solutions, the linear WT model and especially the talin WT model demonstrate much smaller fluctuations, suggesting that local substrate deformations and nonlinear properties of the adapter proteins, such as talin, produce a strong damping effect on system fluctuations, see Figure S3(a), SI. Since this effect was found to take place even in the absence of the force-induced unfolding of the mechanosensitive talin domain [Figure S3(a), SI], the nonlinear force-response of the long talin molecules themselves appears to be sufficient for it to occur.

Further analysis of the long-term stability of such fluctuations showed that it is mainly determined by the relative susceptibility of the cell traction force and the myosin II-pulling force to the actin flow, see Figure S4, SI.

To gain additional insights into the origin of the multistable behaviour of the molecular clutch system, we fitted previously published experimental data on WT MEF cells and MEF Talin 1 KO, Talin 2 shRNA cells treated with myosin II inhibitor, blebbistatin [11], see Figure 3(a-b). Then, using the fitted values of the model parameters, we plotted the cell traction and the myosin II-pulling stress graphs shown in Figures 3(d-f), which showed that the multistable behaviour of cell adhesion may potentially arise due to a cusp-like catastrophe experienced by the molecular clutch system. Specifically, it was found that a decrease in the density of contractile myosin II motors caused by the blebbistatin treatment leads to the appearance of an unstable branch with two saddle-node bifurcation points at its ends, – a typical sign of a cusp catastrophe, see Figures 3(e).

Interestingly, further drop in the density of contractile myosin II motors upon increase of the blebbistatin concentration appeared to lead to the displacement of one of the saddle-node points to infinity, resulting in the formation of the robust bifurcation pattern shown in Figure 3(f). Hence, it can be concluded that, depending on the density of myosin II motors and the elasticity of adapter proteins, there can be two types of cell adhesions on rigid substrates – weak and strong.

From a physical point of view, such bistable behaviour of the molecular clutch system can be understood in terms of the load sharing by molecular clutches. In the case of a low initial density of molecular clutches, they can hardly resist the actin flow generated by myosin II motors, which causes a rapid increase in their mechanical tension and quick dissociation on rigid substrates. This makes it difficult for cells to accumulate a significant amount of adhesion bonds to the substrate, rendering cells into a weak adhesion state. On the other hand, if a cell initially starts with a large number of adhesion bonds, the latter can significantly slow down the flow of actin, with each molecular clutch sharing only a small part of the pulling force generated by myosin II motors. Decrease in the actin flow, in turn, leads to a drop in the build-up rate of the mechanical tension in molecular clutches, allowing the cell to maintain a state of strong adhesion to a rigid substrate over a long period of time. Hence the bistability.

By plotting the stability diagrams for the linear WT and linear KD clutch models, it was further revealed that, in addition to the cusp catastrophe, the molecular clutch system undergoes two more bifurcations associated with the displacement of the saddle-node points to infinity, see Figure 3(c). Both of these bifurcations were also found to be sensitive to the elasticity of the cellular part of molecular clutches and the density of myosin II motors, suggesting that these parameters play an important role in determining the shape of the cell traction curve and thus the mechanosensitive behaviour of cell adhesion.

Notably, the catch-bond behaviour of adhesion receptors (integrins) turned out to be dispensable for the occurrence of all the above bifurcations, since very similar behaviour of the molecular clutch system was also observed in the case of slip-bonds [described by Eq. (11) and Eq. (12)], suggesting that the multistable behaviour is an intrinsic property of this system.

Ligand concentration regulates cell adhesion via a myosin II feedback loop in fibroblast cells

Finally, to investigate the effect of the density of molecular clutches on cell adhesion, we fitted previously published experimental data on WT MEF cells and MEF Talin 1 KO, Talin 2 shRNA cells seeded on elastic sub-

strates that were coated with different fibronectin concentrations [11]. Since the density of fibronectin network affects the rate of molecular clutch formation, as well as the distribution of mechanical load near adhesion sites of molecular clutches, the data fitting was performed by varying the clutch formation rate and the characteristic radius of adhesion sites of molecular clutches. In addition, we also varied the density of myosin II motors as the cell traction curve was found to be highly sensitive to it. Using this approach, the linear clutch model and the talin clutch model were able to fit all the experimental data fairly well, see Figure 4(a,b).

Surprisingly, the data fitting showed a correlation between the density of myosin II motors and the fibronectin concentration. According to the model, the density of myosin II motors pulling on actin filaments decreases by $\sim 30\%$ on substrates coated with 1 μg/ml fibronectin solution compared to the case of 100 μg/ml fibronectin solution, see Figure 4(c). To test this model prediction, we transfected NIH-3T3 cells with myosin regulatory light chain (RLC)-GFP [27] and measured the density and the average size of myosin II stacks labelled with this construct as a function of the fibronectin concentration, see Figures 4(d,e). As a control, we also performed similar measurements in HeLa cells, see Figure S5, SI.

It was found that while in HeLa cells myosin II molecules formed more or less uniform assemblies resembling beads on a string [Figure S5, SI], in NIH-3T3 cells they formed more irregular stacks [Figure 4(d)]. More importantly, although the fibronectin concentration was found to have little effect on the density of myosin II stacks in NIH-3T3 cells, it had a strong effect on their average size [Figure 4(e)], which appeared to be in line with the trend predicted by the talin WT model for WT MEF cells [Figure 4(c)]. This phenomenon, however, was not observed in HeLa cells, suggesting that it may be cell type dependent.

DISCUSSION

In this study, we have developed a semi-analytic model of cell adhesion that, by incorporating a physically realistic force-response of adapter proteins, accurately described previously published experimental measurements of the cell traction force and the retrograde actin flow, providing new detailed insights into the mechanosensitive behaviour of living cells.

Using the model developed in our study, we first showed that in addition to the stability of adhesion bonds, the long-term behaviour of cell adhesion is also highly dependent on interplay between the elastic properties of adapter proteins that constitute the cellular part of molecular clutches and local substrate deformations at the adhesion sites of the molecular clutches. It was found that local substrate deformations play a dominant role in determining cell adhesion on compliant substrates (Young's modulus $E \leq 10$ kPa), whereas the elastic properties of adapter proteins mainly affect cell behaviour on rigid substrates ($E > 30$ kPa), see Figure 1(e). On the other hand, the average deformation of the substrate over large areas of cell adhesion, which are usually studied in the traction force experiments, appeared to play a much smaller role in the cell mechanosensing of the surrounding environment.

Furthermore, it was shown that local substrate deformations and nonlinear elastic properties of the adapter proteins, such as talin, produce a strong damping effect on fluctuations experienced by the molecular clutch system, see Figure S3(a). This model prediction is consistent with experimental observations showing the absence of strong fluctuations in the retrograde flow of actin filaments in living cells [8, 11, 23, 25], which contrasts sharply with existing molecular clutch models that predict large fluctuations in the retrograde actin flow [9, 12, 28].

Remarkably, this damping effect of talin was found to be independent from the force-induced unfolding of the talin mechanosensitive domain, mainly originating from the nonlinear force-response of long talin molecules. Combined with the previously proposed force-buffering effect of talin [16], this mechanism could help stabilize force-transmission pathways in living cells against random fluctuations, thus resembling the shock adsorbing function of muscle force-bearing proteins such as titin and dystrophin [29, 30]. This could potentially allow living cells to provide more deterministic behaviour of adhesion complexes, which may be important for precise control of cell migration on plain substrates or through ECM.

It should be noted that although in this study we considered the force-induced unfolding of only one mechanosensitive talin domain (R3), the developed theoretical framework allows full-scale simulation by considering the entire network of folding-unfolding transitions of all talin domains, which strongly affect the elastic properties of talin [16]. In future, by combining such calculations with simulations of the stability of globular domains at the atomic level [31], this may lead to better understanding of how the protein composition of molecular clutches influences the mechanosensitive behaviour of cell adhesion in a context-dependent manner.

Importantly, the semi-analytical nature of the model developed in our study also allowed a detailed analysis of the stability of the molecular clutch system and bifurcations experienced by it, which previously published models based on purely numeric simulations could not do. This analysis showed that the molecular clutch system undergoes a series of bifurcations at the physiologically relevant values of the model parameters, which leads to a high sensitivity of cell adhesion properties to the elastic characteristics of adapter proteins and the density of myosin II motors, see Figures 2, 3. And while the sensitivity of cell adhesion to myosin II density has been previously reported [11], no such an effect has been discussed in regard to the elasticity of adapter proteins.

Moreover, it was found that, depending on the rigid-

ity of the adapter proteins, cells can exhibit bistable behaviour over a wide range of the model parameters, which is manifested by two states of cell adhesion – weak and strong. This phenomenon appears to be reminiscent of the bistable behaviour of cell adhesion in shear flow, which occurs during the leukocyte extravasation and adhesion of malaria-infected erythrocytes to blood vessel walls [32, 33].

Interestingly, it has previously been suggested that during extravasation, leukocytes must rely on a synergistic cooperation between two different types of adhesion receptors: 1) tight adhesion receptors, which form firm bonds with the blood vessel walls, but exhibit strong bistable behaviour, and 2) rolling adhesion bonds, which are weak and highly dynamic, but facilitate the transition of cells from a weak adhesion state to a strong one [32]. Our study points to the possibility that a similar mechanism may also be used by non-transformed MEF cells.

Specifically, results obtained in this study imply that besides the reduced integrin activation, the loss of the traction force on rigid substrates observed in MEF Talin 1 KO, Talin 2 shRNA cells [Figure 1(c)] could be partially attributed to the change in the type of adapter proteins used by cells in molecular clutches that have mechanical properties different from that of talin. I.e., MEF cells appear to rely on at least two different types of molecular clutches – soft (talin-based) and rigid. And while the rigid molecular clutches were predicted to possess bistable behaviour [Figure 3(b)], soft talin-based clutches were found to lack it, see Figure 3(a). Thus, it is tempting to speculate that MEF cells may use talin-based molecular clutches to form nascent adhesion bonds, which may further promote the formation of rigid molecular clutches by allowing the transition of cells from a weak to a strong adhesion state. By measuring the density of substrate-bound rigid molecular clutches in wild-type cells and talin KO cells, it will be possible to test this hypothesis, warranting future study.

Finally, by fitting previously published traction force microscopy data [11], the model predicted the existence of a correlation between the densities of fibronectin and myosin II motors localized near the cell-substrate interface, which was successfully confirmed in our experiments using SIM imaging of myosin II stacks. Namely, it was found that while the density of myosin II stacks does not change much with the fibronectin density, their average size strongly grows in NIH-3T3 cells with increasing fibronectin concentration. This behaviour is likely regulated by Rho kinase (ROCK), which controls assembly of myosin II stacks by phosphorylation of the myosin II light chain. Indeed, fibronectin density has previously been reported to affect ROCK activation in primary bovine pulmonary artery endothelial cells [34], however, the precise molecular mechanisms underlying this regulation of ROCK by fibronectin density remain unknown.

Our observations suggest that such a feedback loop between fibronectin and myosin II density may be cell type-dependent, as it was found in non-transformed NIH-3T3 fibroblast cells but not in transformed HeLa cells. In future, by comparing multiple cell lines, it might be possible to gain detailed insights into the origin of this interesting phenomenon, which has such a distinct effect on the adhesion properties of normal and transformed cells.

AUTHOR CONTRIBUTIONS

P.L. performed experiments. P.L., Q.W. and A.K.E. analysed the data. M.Y. and A.K.E. designed the research and wrote the paper. A.K.E. supervised the study, derived formulas and carried out computations.

ACKNOWLEDGEMENT

We are very grateful to Dr. Jie Yan (MBI, Singapore) and Dr. Alexander D. Bershadsky (MBI, Singapore) for insightful discussion of the results of our study. Also, we would like to thank Dr. Alexander D. Bershadsky for providing genetic constructs used in the study, and Dr. Qin Peng (Shenzhen Bay Laboratory, China) for NIH-3T3 and HeLa cell lines. We would like to thank Shenzhen Bay Laboratory Supercomputing Center for assistance in carrying out the calculations and Bioimaging Core of Shenzhen Bay Laboratory for providing imaging support. We also would like to thank Bioimaging Core engineer Yu Mei for assistance with SIM microscopy (Elyra7). This work was supported by the start-up funds from Shenzhen Bay Laboratory (A.K.E.).

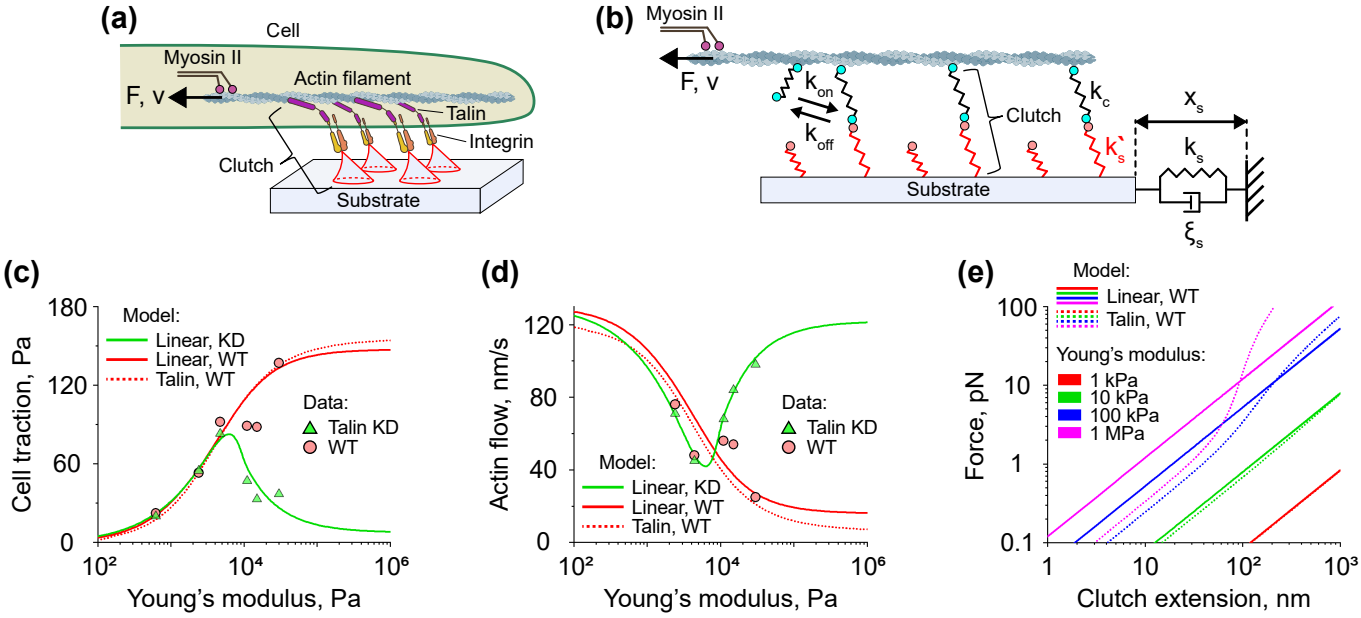

FIG. 1. **Molecular clutch mechanism.** **(a)** Integrins and talins are the main components of adhesion links that form between the actin cytoskeleton and the substrate. Myosin II-induced retrograde flow of actin filaments leads to mechanical stretching of these links, causing local substrate deformations (shown in red). Force-transmitting units, each including a cellular part (integrin and talin) and an extracellular part (locally deformed substrate), are referred to in this study as 'molecular clutches'. **(b)** In the model, molecular clutches were represented by composite springs consisting of two parts – a cellular one (k_c) and an extracellular one (k_s'). While latter was assumed to have a linear response to the applied load, the former was considered as a linear spring in the linear clutch model and a nonlinear spring with a talin-like force-response in the talin clutch model. Kinetic behaviour of molecular clutches under mechanical load was described by their formation and dissociate rates, k_{on} and k_{off}, respectively. The total average deformation of the substrate (x_s) over a large cell adhesion area encompassing many molecular clutches was represented in the model by a linear spring with the stiffness k_s. Viscous properties of the substrate were described in the model by the constant ξ_s. **(c, d)** Fitting of the cell traction and the actin flow experimental data to the linear clutch model (solid curves) and to the talin clutch model (dotted curves). To this aim, we used experimental data collected on WT MEF cells (red circles) and MEF Talin 1 KO, Talin 2 shRNA cells (green triangles) taken from ref. [11]. The fitted values of the model parameters are shown in Table 1, SI. **(e)** Force-extension curves of linear molecular clutches (solid lines) and nonlinear talin clutches (dotted curves) at different values of the substrate Young's modulus.

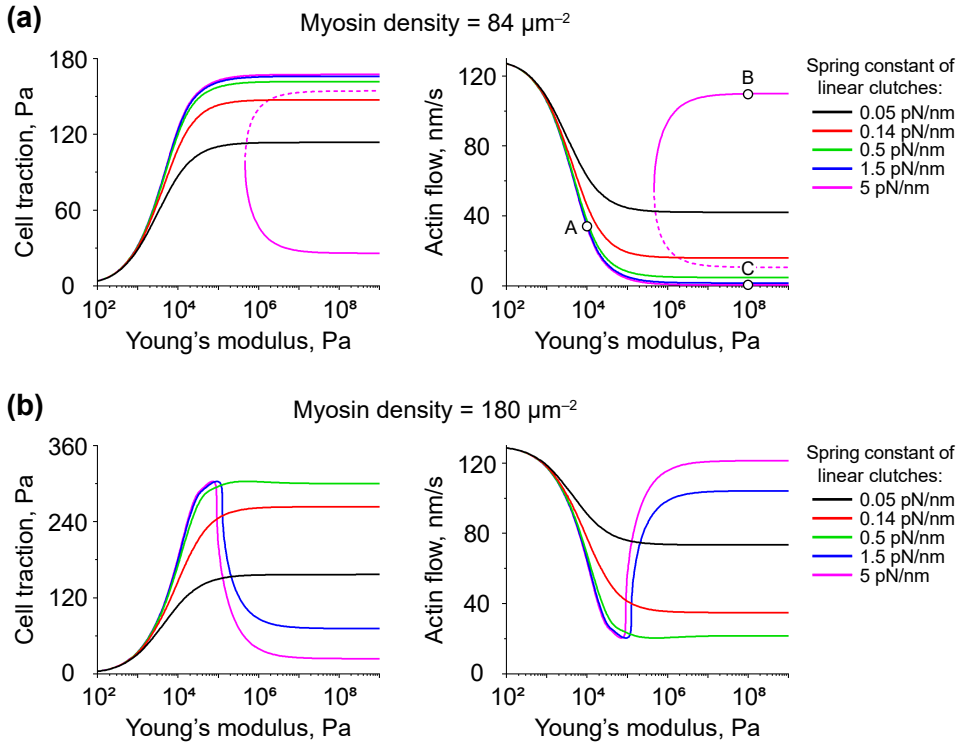

FIG. 2. **Effect of the cellular part of molecular clutches on cell adhesion. (a, b)** Graphs of the cell traction curves and the actin flow curves calculated using the linear clutch model for various values of the spring constant k_c, which describes the elastic properties of the cellular part of molecular clutches. Two different densities of myosin II motors, 84 μm^{-2} (a) and 180 μm^{-2} (b), were used in the calculations. It can be seen from the figure that the stiffness of the cellular part of molecular clutches has a strong effect on the cell adhesion properties in the case of rigid substrates (Young's modulus $>$ 10 kPa), while there are almost no changes on soft substrates (Young's modulus $<$ 10 kPa). In addition, the figure shows that in the case of stiff molecular clutches [k_c = 5 pN/nm, panel(a)], the system undergoes a bifurcation, which results in bistable behaviour of the cell traction curve and the actin flow curve on rigid substrates. For points A, B and C shown in the right panel (a), we performed stochastic simulations, which confirmed that the molecular clutch system exhibits bistable behaviour at high values of the substrate Young's modulus, but not at low values, see Figure S3(b), SI. In the calculations, all values of the model parameters, except of the clutch stiffness and myosin II density, were the same as in the linear WT model, see Table 1, SI. In the figure, the solid curves denote stable branches of the graphs corresponding to stable system fluctuations around the stationary solutions of Eq. (6), whereas dashed curves indicate unstable branches, see Figure S4, SI for more details.

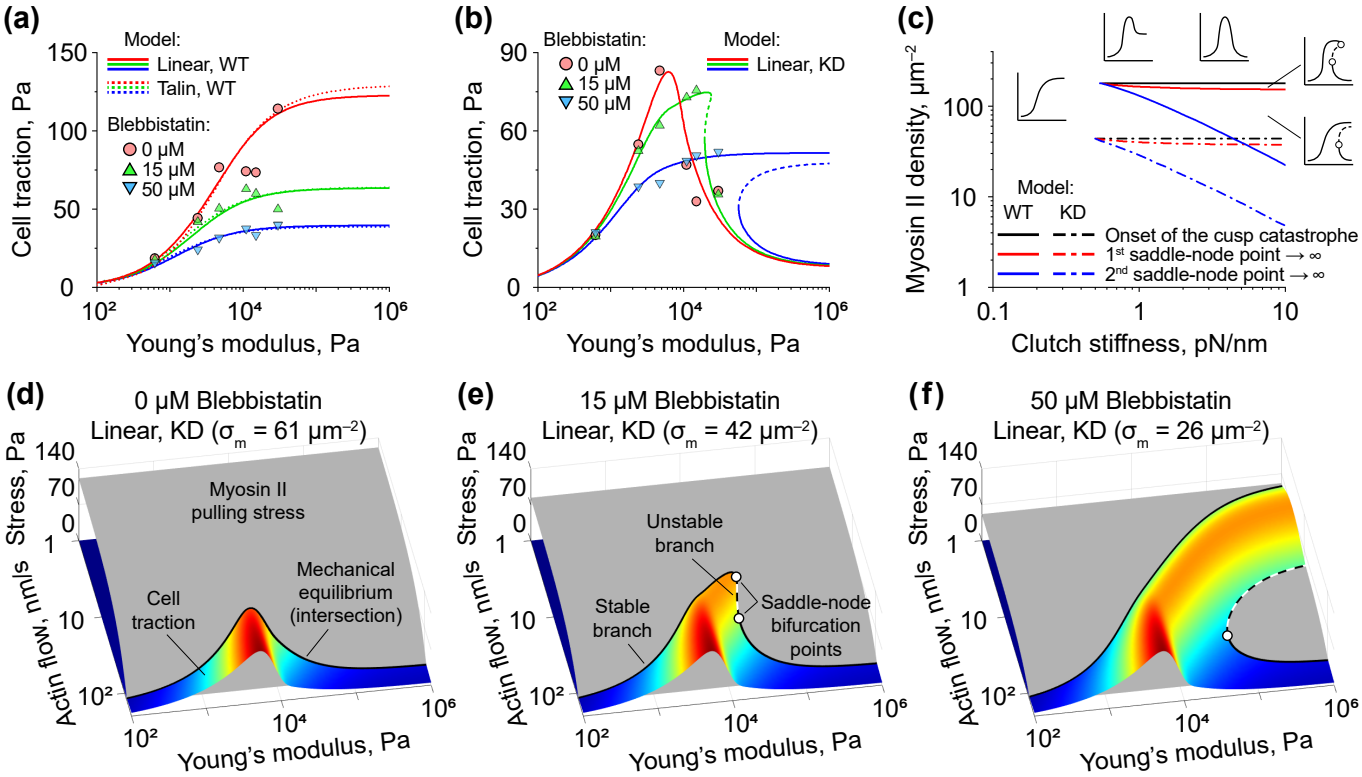

FIG. 3. **Role of myosin II density in cell adhesion.** **(a, b)** Fitting of experimental data collected on WT MEF cells (a) and MEF Talin 1 KO, Talin 2 shRNA cells (b) treated with different concentrations of blebbistatin [11]. The data were fitted to the linear clutch model (solid curves) and talin clutch model (dotted curves) by varying only the density of myosin II motors. The rest of the model parameters were fixed at the values shown in Table 1, SI. The dashed segments of the cell traction curves obtained by using the linear clutch model indicate unstable branches of the corresponding graphs. **(c)** Stability diagrams of the linear molecular clutch model calculated for the two sets of the model parameter values obtained by fitting the experimental data shown in panels (a) and (b). Onsets of the cusp catastrophe (black curve) and the displacements of the first and the second saddle-node points to infinity (red curve and blue curve, respectively) are shown in the plot. Pictograms schematically indicate the characteristic profiles of the cell traction curve in the corresponding regions of the stability diagram. **(d-f)** 3D plots of the cell traction stress (coloured surface) and myosin II-pulling stress (gray surface) calculated for MEF Talin 1 KO, Talin 2 shRNA cells treated with different concentrations of myosin II inhibitor, blebbistatin. The black solid curves indicate stable branches of the system formed by the intersection of the two surfaces, whereas the black dashed lines indicate unstable branches, see Figure S4, SI for more details. White dots designate saddle-node bifurcation points.

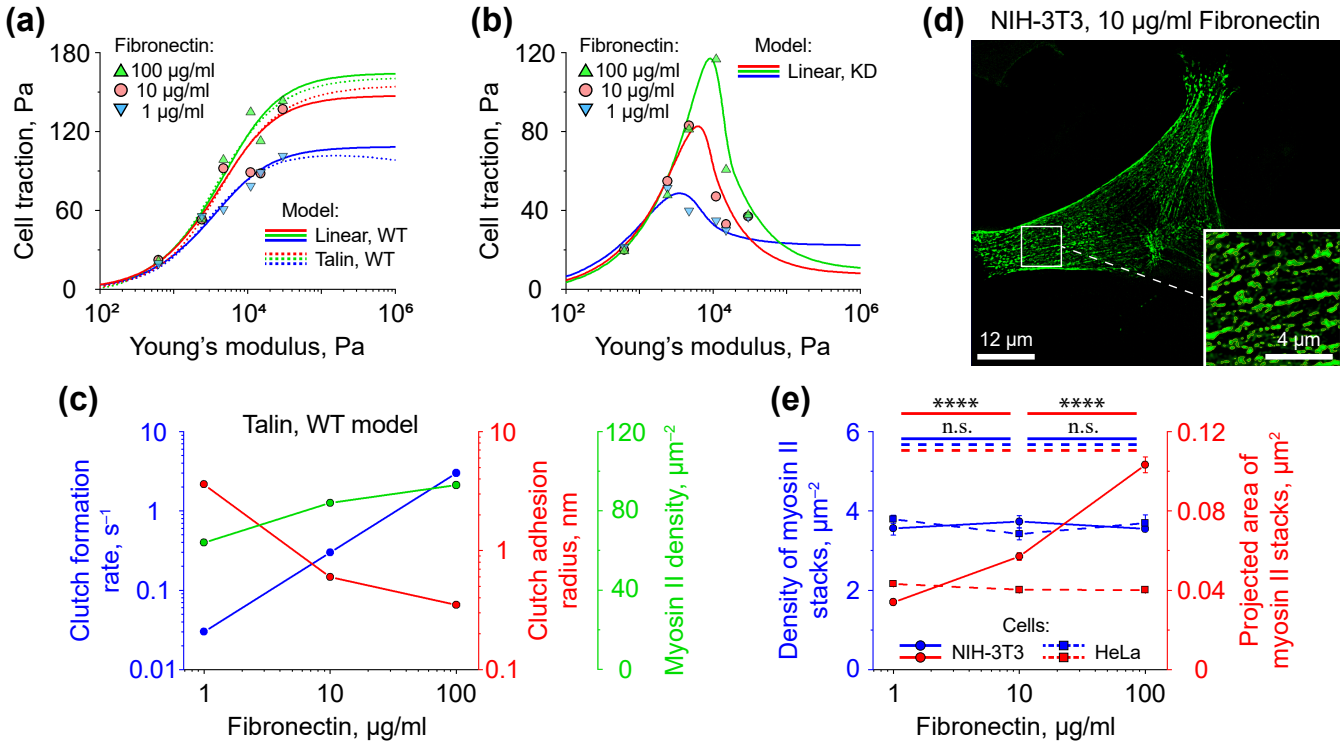

FIG. 4. **Effect of the fibronectin density on cell adhesion. (a, b)** Fitting of experimental data collected on WT MEF cells (a) and MEF Talin 1 KO, Talin 2 shRNA cells (b) at different concentrations of fibronectin solution used to coat the substrate surface [11]. The data were fitted to the linear clutch model (solid curves) and talin clutch model (dotted curves) by varying the rate of clutch formation, the radius of adhesion sites of molecular clutches, and the density of myosin II motors. The rest of the model parameters were fixed at the values shown in Table 1, SI. **(c)** Values of the fitted model parameters depending on the fibronectin concentration. **(d)** SIM image of a NIH-3T3 fibroblast cell expressing myosin RLC-GFP seeded on a glass slide coated with 10 μg/ml fibronectin solution. The inset shows the enlarged area indicated by the white square in the figure. **(e)** Measured density (blue curve) and the projected area (red curve) of myosin II stacks labelled with RLC-GFP in NIH-3T3 and HeLa cells as a function of the fibronectin concentration used to coat slides. Each data point shows the mean calculated from $N = 770 - 2558$ myosin II stacks, errorbars represent SEM. The bars above the graphs indicate pairwise statistical difference between the points of the corresponding plots (n.s. – non-significant, $****$ – $p < 0.0001$).

[1] V. Vogel and M. Sheetz, Local force and geometry sensing regulate cell functions., Nat. Rev. Mol. Cell Biol. **7**, 265 (2006).

[2] H. Wolfenson, B. Yang, and M. P. Sheetz, Steps in mechanotransduction pathways that control cell morphology., Annu. Rev. Physiol. **81**, 585 (2019).

[3] H. T. Nia, L. L. Munn, and R. K. Jain, Physical traits of cancer., Science **370**, eaaz0868 (2020).

[4] S. W. Moore, P. Roca-Cusachs, and M. P. Sheetz, Stretchy proteins on stretchy substrates: the important elements of integrin-mediated rigidity sensing., Dev. Cell **19**, 194 (2010).

[5] A. K. Efremov, M. Yao, Y. Sun, Y. H. Tee, M. P. Sheetz, A. D. Bershadsky, B. Martinac, and J. Yan, Application of piconewton forces to individual filopodia reveals mechanosensory role of L-type Ca^{2+} channels., Biomaterials **284**, 121477 (2022).

[6] A. E. M. Beedle and S. Garcia-Manyes, The role of single-protein elasticity in mechanobiology., Nat. Rev. Mater. **8**, 10 (2023).

[7] T. Mitchison and M. Kirschner, Cytoskeletal dynamics and nerve growth., Neuron **1**, 761 (1988).

[8] C. E. Chan and D. J. Odde, Traction dynamics of filopodia on compliant substrates., Science **322**, 1687 (2008).

[9] B. L. Bangasser and D. J. Odde, Master equation-based analysis of a motor-clutch model for cell traction force., Cell Mol. Bioeng. **6**, 449 (2013).

[10] A. Elosegui-Artola, E. Bazellières, M. D. Allen, I. Andreu, R. Oria, R. Sunyer, J. J. Gomm, J. F. Marshall, J. L. Jones, X. Trepat, and P. Roca-Cusachs, Rigidity sensing and adaptation through regulation of integrin types., Nat. Mater. **13**, 631 (2014).

[11] A. Elosegui-Artola, R. Oria, Y. Chen, A. Kosmalska, C. Pérez-González, N. Castro, C. Zhu, X. Trepat, and P. Roca-Cusachs, Mechanical regulation of a molecular clutch defines force transmission and transduction in response to matrix rigidity., Nat. Cell Biol. **18**, 540 (2016).

[12] Z. Gong, S. E. Szczesny, S. R. Caliari, E. E. Charrier, O. Chaudhuri, X. Cao, Y. Lin, R. L. Mauck, P. A. Janmey, J. A. Burdick, and V. B. Shenoy, Matching material and cellular timescales maximizes cell spreading on viscoelastic substrates., Proc. Natl. Acad. Sci. U.S.A. **115**, E2686 (2017).

[13] C. E. Chan and D. J. Odde, Traction dynamics of filopodia on compliant substrates, Science **322**, 1687 (2008).

[14] M. Yao, W. Qiu, R. Liu, A. K. Efremov, P. Cong, R. Seddiki, M. Payre, C. T. Lim, B. Ladoux, R.-M. Mège, and J. Yan, Force-dependent conformational switch of α-catenin controls vinculin binding., Nat. Commun. **5**, 4525 (2014).

[15] M. Yao, B. T. Goult, H. Chen, P. Cong, M. P. Sheetz, and J. Yan, Mechanical activation of vinculin binding to talin locks talin in an unfolded conformation., Sci. Rep. **4**, 4610 (2014).

[16] M. Yao, B. T. Goult, B. Klapholz, X. Hu, C. P. Toseland, Y. Guo, P. Cong, M. P. Sheetz, and J. Yan, The mechanical response of talin., Nat. Commun. **7**, 11966 (2016).

[17] T. Shimada, M. Toriyama, K. Uemura, H. Kamiguchi, T. Sugiura, N. Watanabe, and N. Inagaki, Shootin1 interacts with actin retrograde flow and L1-CAM to promote axon outgrowth., J. Cell Biol. **181**, 817 (2008).

[18] Z. Zhao, S. H. Tan, H. Machiyama, K. Kawauchi, K. Araki, H. Hirata, and Y. Sawada, Association between tensin 1 and p130Cas at focal adhesions links actin inward flux to cell migration., Biol. Open **5**, 499 (2016).

[19] A. Clarke, P. G. McQueen, H. Y. Fang, R. Kannan, V. Wang, E. McCreedy, S. Wincovitch, and E. Giniger, Abl signaling directs growth of a pioneer axon in *Drosophila* by shaping the intrinsic fluctuations of actin., Mol. Biol. Cell **31**, 466 (2020).

[20] L. M. Owen, N. A. Bax, W. I. Weis, and A. R. Dunn, The C-terminal actin-binding domain of talin forms an asymmetric catch bond with F-actin., Proc. Natl. Acad. Sci. U.S.A. **119**, e2109329119 (2022).

[21] J. Neumann and K.-E. Gottschalk, The integrin-talin complex under force., Protein Eng. Des. Sel. **29**, 503 (2016).

[22] F. Kong, A. J. García, A. P. Mould, M. J. Humphries, and C. Zhu, Demonstration of catch bonds between an integrin and its ligand., J. Cell Biol. **185**, 1275 (2009).

[23] N. O. Alieva, A. Efremov, S. Hu, D. Oh, Z. Chen, M. Natarajan, H. T. Ong, A. Jégou, G. Romet-Lemonne, J. T. Groves, M. P. Sheetz, J. Yan, and A. D. Bershadsky, Myosin IIA and formin dependent mechanosensitivity of filopodia adhesion., Nat. Commun. **10**, 3593 (2019).

[24] M. Ghibaudo, A. Saez, T. Léa, A. Xayaphoummine, J. Browaeys, P. Silberzan, A. Buguinb, and B. Ladoux, Traction forces and rigidity sensing regulate cell functions., Soft Matter **4**, 1836 (2008).

[25] T. Bornschlögl, S. Romero, C. L. Vestergaard, J.-F. Joanny, G. Tran Van Nhieu, and P. Bassereau, Filopodial retraction force is generated by cortical actin dynamics and controlled by reversible tethering at the tip., Proc. Natl. Acad. Sci. U.S.A. **110**, 18928 (2013).

[26] D. Riveline, E. Zamir, N. Q. Balaban, U. S. Schwarz, T. Ishizaki, S. Narumiya, Z. Kam, B. Geiger, and A. D. Bershadsky, Focal contacts as mechanosensors: externally applied local mechanical force induces growth of focal contacts by an mDia1-dependent and ROCK-independent mechanism., J. Cell Biol. **153**, 1175 (2001).

[27] S. Hu, K. Dasbiswas, Z. Guo, Y.-H. Tee, V. Thiagarajan, P. Hersen, T.-L. Chew, S. A. Safran, R. Zaidel-Bar, and A. D. Bershadsky, Long-range self-organization of cytoskeletal myosin II filament stacks., Nat. Cell Biol. **19**, 133 (2017).

[28] R. Alonso-Matilla, P. P. Provenzano, and D. J. Odde, Optimal cell traction forces in a generalized motor-clutch model., Biophys. J. (2023).

[29] H. Chen, G. Yuan, R. S. Winardhi, M. Yao, I. Popa, J. M. Fernandez, and J. Yan, Dynamics of equilibrium folding and unfolding transitions of titin immunoglobulin domain under constant forces., J. Am. Chem. Soc. **137**, 3540 (2015).

[30] S. Le, M. Yu, L. Hovan, Z. Zhao, J. Ervasti, and J. Yan, Dystrophin as a molecular shock absorber., ACS Nano **12**, 12140 (2018).

[31] S. Guo, Q. Tang, M. Yao, H. You, S. Le, H. Chen, and J. Yan, Structural–elastic determination of the force-dependent transition rate of biomolecules., Chem. Sci. **9**, 5871 (2018).

[32] A. Efremov and J. Cao, Bistability of cell adhesion in shear flow., Biophys. J. **101**, 1032 (2011).

[33] X. Xu, A. K. Efremov, A. Li, L. Lai, M. Dao, C. T. Lim, and J. Cao, Probing the cytoadherence of malaria infected red blood cells under flow., PLoS One **8**, e64763 (2013).

[34] K. Bhadriraju, M. Yang, S. A. Ruiz, D. Pirone, J. Tan, and C. S. Chen, Activation of ROCK by RhoA is regulated by cell adhesion, shape, and cytoskeletal tension., Exp. Cell Res. **313**, 3616 (2007).